


RESEARCH

Open Access



# The role of oxidative stress-mediated fibro-adipogenic progenitor senescence in skeletal muscle regeneration and repair

Yuqing Yao<sup>1†</sup>, Yusheng Luo<sup>1,3†</sup>, Xiaomei Liang<sup>1,4†</sup>, Li Zhong<sup>1,3†</sup>, Yannan Wang<sup>5</sup>, Zhengchao Hong<sup>6</sup>, Chao Song<sup>7</sup>, Zeyu Xu<sup>5</sup>, Jiancheng Wang<sup>1,3\*</sup>  and Miao Zhang<sup>2\*</sup>

## Abstract

**Background** Stem cells play a pivotal role in tissue regeneration and repair. Skeletal muscle comprises two main stem cells: muscle stem cells (MuSCs) and fibro-adipogenic progenitors (FAPs). FAPs are essential for maintaining the regenerative milieu of muscle tissue and modulating the activation of muscle satellite cells. However, during acute skeletal muscle injury, the alterations and mechanisms of action of FAPs remain unclear.

**Methods** we employed the GEO database for bioinformatics analysis of skeletal muscle injury. A skeletal muscle injury model was established through cardiotoxin (CTX, 10 μM, 50 μL) injection into the tibialis anterior (TA) of C57BL/6 mice. Three days post-injury, we extracted the TA, isolated FAPs (CD31<sup>-</sup>CD45<sup>-</sup>PDGFRα<sup>+</sup>Sca-1<sup>+</sup>), and assessed the senescence phenotype through SA-β-Gal staining and Western blot. Additionally, we established a co-culture system to evaluate the capacity of FAPs to facilitate MuSCs differentiation. Finally, we alleviated the senescent of FAPs through in vitro (100 μM melatonin, 5 days) and in vivo (20 mg/kg/day melatonin, 15 days) administration experiments, confirming melatonin's pivotal role in the regeneration and repair processes of skeletal muscle.

**Results** In single-cell RNA sequencing analysis, we discovered the upregulation of senescence-related pathways in FAPs following injury. Immunofluorescence staining revealed the co-localization of FAPs and senescent markers in injured muscles. We established the CTX injury model and observed a reduction in the number of FAPs post-injury, accompanied by the manifestation of a senescent phenotype. Melatonin treatment was found to attenuate the injury-induced senescence of FAPs. Further co-culture experiments revealed that melatonin facilitated the restoration of FAPs' capacity to promote myoblast differentiation. Through GO and KEGG analysis, we found that the administration of melatonin led to the upregulation of AMPK pathway in FAPs, a pathway associated with antioxidant stress response. Finally, drug administration experiments corroborated that melatonin enhances skeletal muscle regeneration and repair by alleviating FAP senescence in vivo.

<sup>†</sup>Yuqing Yao, Yusheng Luo, Xiaomei Liang and Li Zhong contributed equally to this work.

\*Correspondence:  
Jiancheng Wang  
wangjch38@mail.sysu.edu.cn  
Miao Zhang  
zhangm87@mail.sysu.edu.cn

Full list of author information is available at the end of the article



© The Author(s) 2025. **Open Access** This article is licensed under a Creative Commons Attribution-NonCommercial-NoDerivatives 4.0 International License, which permits any non-commercial use, sharing, distribution and reproduction in any medium or format, as long as you give appropriate credit to the original author(s) and the source, provide a link to the Creative Commons licence, and indicate if you modified the licensed material. You do not have permission under this licence to share adapted material derived from this article or parts of it. The images or other third party material in this article are included in the article's Creative Commons licence, unless indicated otherwise in a credit line to the material. If material is not included in the article's Creative Commons licence and your intended use is not permitted by statutory regulation or exceeds the permitted use, you will need to obtain permission directly from the copyright holder. To view a copy of this licence, visit <http://creativecommons.org/licenses/by-nc-nd/4.0/>.

**Conclusion** In this study, we first found FAPs underwent senescence and redox homeostasis imbalance after injury. Next, we utilized melatonin to enhance FAPs regenerative and repair capabilities by activating AMPK signaling pathway. Taken together, this work provides a novel theoretical foundation for treating skeletal muscle injury.

**Keywords** FAPs, Skeletal muscle injury, Senescence, Melatonin

## Introduction

Stem cells are crucial for maintaining tissue homeostasis and facilitating regeneration following injury [1]. Among the various organ systems, skeletal muscle has garnered considerable research interest due to its mechanisms for homeostasis maintenance and regenerative responses after injury [2–4]. These regenerative processes predominantly depend on resident MuSCs [5, 6], commonly referred to as satellite cells, as well as FAPs [7, 8].

Notably, cytokine networks, growth factors, and extracellular matrix components within the skeletal muscle microenvironment play pivotal roles in regulating myocyte differentiation, proliferation, and regenerative processes [9]. During the regeneration process, MuSCs act as the primary regenerative agents. In their physiological quiescent state, MuSCs are located beneath the basal lamina of myofibers, but they become activated in response to injury [10–12], which is precisely regulated by paracrine signaling from niche components including FAPs and other cellular constituents within the microenvironment [13]. Concurrently, FAPs—multipotent stromal cells characterized by PDGFR $\alpha$ <sup>+</sup>/Sca-1<sup>+</sup> expression and specific to muscle tissue [14–16]—exhibit temporally regulated dynamic responses. They initiate rapid proliferation and migration to injury sites during the early phases of injury [17, 18] and secrete trophic factors such as IGF-1 and IL-6, which promote MuSC proliferation and differentiation [19]. Disruption of this homeostatic process, particularly functional decline in FAPs, may lead to impaired tissue repair [13]. However, the mechanistic basis underlying FAPs' functional deterioration triggered by microenvironmental perturbations remains to be elucidated [20, 21].

When selecting injury models, chemical induction methods are frequently employed due to their high reproducibility and standardized protocols ([22]. The CTX injection model is particularly noteworthy for inducing reversible damage by specifically disrupting myocyte calcium homeostasis ([23]. In comparison to the NTX/BaCl<sub>2</sub> models, which are associated with vascular damage, or mechanical models characterized by uncontrollable variables [24], the CTX model offers significant advantages in minimizing neurovascular side effects. Consequently, it is regarded as the preferred experimental system for investigating mechanisms of acute muscle regeneration.

Our investigation focused on deciphering the mechanism of decline of the function of FAPs. ScRNA-seq

initially uncovered prominent senescence characteristics within this cell population during injury progression. Mechanistic studies demonstrated that oxidative stress primarily induced cellular senescence and dysfunction through ROS overproduction in damaged cells. Building upon these observations, we demonstrated that antioxidant compounds could reactivate FAPs functionality via AMPK pathway-mediated ROS metabolism reprogramming. This study not only enhances the mechanistic understanding of muscle regeneration dynamics, but also offers novel therapeutic perspectives for skeletal muscle repair strategies.

## Materials and methods

### Animals

C57BL/6J mice (7 weeks old) were purchased from Shenzhen LingFu TopBiotech. Co., LTD., (Shenzhen, China) and acclimatized for at least 5 days upon arrival. Under a 12:12 h light: dark cycle, mice are housed individually and provided with food and water ad libitum. Animal care and use procedures are carried out in accordance with the standards outlined in the Guidelines for the Care and Use of Laboratory Animals, which are reviewed and approved by the Laboratory Animal Management and Use Committee of Shenzhen LingFu TopBiotech. Co., LTD.,. The ethics approval number is: TOPGM-IACUC-2023-0200.

### Acute skeletal muscle injury and melatonin in vivo treatment model

To induce muscle injury, mice were anesthetized using a gas anesthesia system for small animals, with isoflurane (R510-22, RWD LIFE SCIENCE, China) introduced into the vaporizer to achieve a suitable concentration of 3% isoflurane for induction. After anesthetizing the mice, they were transferred to a heating pad and maintained under continuous inhalation of 1% isoflurane. Cardiotoxin (CTX, 10  $\mu$ M, 50  $\mu$ L) was injected multiple times into the tibialis anterior (TA) muscle of the mice ([25]. Following the injection, the mice were returned to their cages and monitored until they woke up. Three days post-injury, confirming successful modeling, subsequent experiments were conducted.

For the treatment models, eighteen C57BL/6J mice were divided into 3 groups, with 6 mice in each group. The “Control group” (sham operation group) received an intramuscular injection of 50  $\mu$ L PBS; the “Injury + Ethanol group” (placebo treatment for the injury model) received an intramuscular injection of 10

$\mu\text{M}$ , 50  $\mu\text{L}$  CTX, and began intraperitoneal injection of 5% ethanol 3 days after modeling, lasting for 15 days; the **“Injury + Melatonin group”** (melatonin treatment for the injury model) received an intramuscular injection of 10  $\mu\text{M}$ , 50  $\mu\text{L}$  CTX, and began intraperitoneal injection of 20 mg/kg/day melatonin 3 days after modeling, lasting for 15 days ([26]). The animals were euthanized by cervical dislocation under isoflurane anesthesia, and the TA was collected.

#### Single cell sequencing data analysis

The data is obtained from database GSE214892(*GEO Accession viewer (nih.gov)*). Raw sequencing reads were first processed using Cell Ranger to perform alignment, filtering, and UMI counting, generating a gene-barcode matrix. The quality of the cells was assessed, and low-quality cells or doublets were removed based on total UMI counts. The gene expression matrix was then normalized and log-transformed. Principal component analysis (PCA) was conducted to reduce dimensionality, followed by clustering using Louvain algorithm and visualization using UMAP ([27]). Differential gene expression analysis was performed between clusters using Seurat to identify marker genes. Pathway enrichment analysis was conducted using GSEA to interpret the biological significance of the identified genes. The cell types were annotated by comparing marker genes to known cell-type signatures from the literature ([28]).

#### Transcriptome sequencing analysis

The data was obtained from database GSE214008. Differential expression analysis was performed using DESeq2 and EdgeR, with criteria for significance, adjusted  $p\text{-value} < 0.05$ , fold change  $> 2$  ([29]). Functional enrichment analysis of differentially expressed genes was conducted using Gene Ontology (GO) analysis and Kyoto Encyclopedia of Genes and Genomes (KEGG) pathway analysis to identify significant biological pathways associated with the observed expression changes ([30, 31]).

#### Fresh frozen muscle technique

An OCT compound was applied to a piece of cork. To obtain cross-sections of the muscle, the distal tendon was inserted, and about 3/4 of the muscle was left exposed. The TA was then embedded in OCT, ensuring the muscle was in a vertical position relative to the cork. The cork with the muscle was quickly immersed in liquid nitrogen for rapid freezing, left for one minute, and then stored at  $-20^\circ\text{C}$ . The temperature of the cryostat was set to  $-20$  to  $-22^\circ\text{C}$ , and the blade and sample were placed in the cryostat to equilibrate for at least 30 min. The section thickness of the instrument was set to 10  $\mu\text{m}$ , and tissue sections were cut. After sectioning, the slides were stored at  $-20^\circ\text{C}$ .

#### Muscle tissue Immunofluorescence

Muscle sections were fixed with 4% paraformaldehyde (PFA), and antigen retrieval was conducted using a Tris-EDTA buffer solution (comprising 1.21 g of Tris and 0.37 g of EDTA per liter of double-distilled water, adjusted to pH 9.0). The sections were permeabilized with 0.5% Triton X-100 for 10 min, followed by blocking with a blocking buffer containing 5% goat serum for 1 h. Subsequently, the primary antibody was incubated overnight at  $4^\circ\text{C}$  (p16: sc-1661, Santa Cruz, TX, USA; p21: sc-6246, Santa Cruz, TX, USA; PDGFR $\alpha$ : 3174T, Cell Signaling Technology, MA, USA). The secondary antibody (A-11008/A-21235, Thermofisher, CA, USA) was then incubated at room temperature for 1 h in a dark room. Nuclei were counterstained using DAPI-containing mounting media (F6057, Sigma-Aldrich, MO, USA). Observations and imaging were performed using the DragonflyCR-DFLY (TE, Andor Dragonfly CR-DFLY-202-2540). The mean fluorescence intensity (MFI) of p16 or p21 in the region was quantified using ImageJ.

#### Masson trichrome staining

Masson trichrome staining was conducted using the Masson Trichrome Staining Kit (G1006, Servicebio, Wuhan, China) on 10  $\mu\text{m}$  frozen sections of tibialis anterior (TA) muscle. The sections were initially fixed in 95% ethanol for 20 min. Subsequently, they were incubated with the solutions provided in the Masson Trichrome Staining Kit. Following staining, the sections underwent dehydration in 95% ethanol for 10 s, were rinsed twice with anhydrous ethanol for 10 s each, and then washed twice with xylene for 1 min each. The sections were mounted with neutral balsam to facilitate imaging and fibrosis quantification. Quantification of TA muscle fibrosis was performed using ImageJ software, with the collagen volume fraction determined as the ratio of collagen-positive (blue-stained) areas to the total tissue area.

#### Sirius red staining

A modified Sirius Red staining kit (G1078-100ML, Servicebio, Wuhan, China) was employed for the staining of muscle tissue. Following deparaffinization, muscle sections were immersed in Sirius Red Staining Solution A and incubated in a  $65^\circ\text{C}$  oven for 30 min. The sections were then rinsed with water until the yellow coloration diminished, after which they were immersed in Sirius Red Staining Solution B for 2 min. Subsequently, the sections were rinsed with water again and immersed in Sirius Red Staining Solution C for 30 min. A brief rinse with water (1–2 s) was performed, followed by rapid dehydration through immersion in three separate cylinders of absolute ethanol for 3 s each. The sections were then placed in clean xylene for 5 min for clearing, after which they were mounted with neutral balsam. Imaging and

quantification of fibrosis were conducted using Image Pro Plus software, which calculated the collagen fiber area fraction as the ratio of the collagen fiber-positive red region to the total tissue area.

#### **Glycogen PAS staining**

The glycogen content in muscle tissue was quantified utilizing a glycogen assay kit (G1008, Servicebio, Wuhan, China) in accordance with the manufacturer's instructions. Additionally, periodic acid–Schiff (PAS) staining was employed. For PAS staining, a series of frozen sections were prepared from fresh tissue and fixed with ice-cold acetone for 5 min. Following natural air-drying, the sections were treated with potassium periodate solution for 10 min and subsequently rinsed with water for 5 min. Schiff's solution was then applied, and the sections were rinsed with water for 10 min before being stained for 15 min. Nuclear counterstaining was conducted using hematoxylin. ImageJ software was utilized for statistical analysis, and the glycogen volume fraction was determined by calculating the ratio of the glycogen-positive area to the total tissue area.

#### **Isolation of primary FAPs**

The mice were euthanized via cervical dislocation and subsequently immersed in 75% ethanol for 5 min. The lower limb muscles were rapidly excised, with all adipose tissue, fascia, and other extraneous tissues meticulously removed. The muscle tissue was longitudinally sectioned to approximately 1 mm in thickness and transferred to a collagenase solution. This preparation was agitated at 180 rpm on a shaker at 37 °C for 1 h. Post-digestion, the tissue was transferred to a sterile environment, and digestion was halted using pre-cooled PBS at a volume ten times that of the original. The solution was sequentially filtered through 100 µm and 70 µm membranes, followed by centrifugation at room temperature at 1200 rpm for 5 min, after which the supernatant was discarded. The pellet was rinsed once with PBS, and the supernatant was discarded again. The cells were then resuspended in a basal DMEM/F12 complete medium, supplemented with 2% penicillin/streptomycin and 10% fetal bovine serum, and cultured in a 10 cm culture dish. After 4–6 h, the medium was replaced with fresh complete medium, and incubation continued. Approximately 8 h later, the medium was changed again.

#### **Identification of FAPs by flow cytometry**

The single-cell suspension was incubated with purified anti-CD16/CD32 antibodies (clone 2.4G2, Sungene Biotech, Tianjin, China) for 15 min to block the Fc receptor. Following a washing step, the cells were incubated with FITC-conjugated anti-mouse CD45 (103107, Biolegend,

CA, USA), PE-conjugated anti-mouse/human CD31 (561073, BD Biosciences, NJ, USA), APC-conjugated anti-mouse PDGFRα (135907, Biolegend, CA, USA), and V450-PB450-conjugated anti-mouse Sca-1 (108127, Biolegend, CA, USA) at 4 °C for 30 min in the dark. After another washing step, 300 µl of 3% BSA was added to each tube to resuspend the cells. The samples were then analyzed by flow cytometry using the Cytotflex LX system, and the data was processed with FlowJo software (version 10.8.1) ([32]).

#### **Melatonin in vitro treatment model**

Primary FAPs isolated from the injury group mice were utilized to develop this experimental model. Melatonin (M5250, Sigma-Aldrich, St. Louis, MO) was initially dissolved in anhydrous ethanol to create a stock solution with a concentration of 100 mM. This stock solution was subsequently diluted in the basal medium to achieve a final concentration of 100 µM for application in cell treatment. The extracted primary FAPs from the injury group mice were seeded into six-well plates. Upon reaching a cell density of 60%, the treatment group was exposed to a medium supplemented with melatonin, whereas the control group was administered an equivalent volume of anhydrous ethanol at the same concentration. This incubation process was maintained for a duration of five days ([33]).

#### **Assessment of creatine kinase (CK) and lactate dehydrogenase (LDH) enzymatic activity**

The activities of CK and LDH were quantified utilizing the Creatine Kinase Assay Kit (A032-1-1, Nanjing Jiancheng Bio, Nanjing, China) and the Lactate Dehydrogenase Assay Kit (A020-1-2, Nanjing Jiancheng Bio, Nanjing, China), respectively. Serum was extracted from mice, and the samples were prepared following the protocols provided by the manufacturer. Absorbance changes for each sample were recorded at wavelengths of 660 nm and 440 nm using a microplate reader. The enzymatic activities of CK and LDH in the serum were subsequently determined by referencing a standard curve.

#### **Senescence-associated β-galactosidase (SA-β-Gal) staining**

SA-β-Gal staining was conducted utilizing the Senescence-Related β-Galactosidase Staining Kit (C0602, Beyotime, Shanghai, China). To initiate the staining process, 1 ml of β-galactosidase staining fixative solution was added to FAPs cultured in control, injury, and melatonin-treated groups within six-well plates, followed by a 15-minute fixation period at room temperature. Subsequent to three washes, 1 ml of a working solution containing 0.05 mg/ml X-galactosidase was applied to the cells, which were then incubated overnight at 37 °C in the



dark. The cells were subsequently examined using a light microscope (TE2000-S; Nikon, Tokyo, Japan). The catalytic activity of the senescence-specific  $\beta$ -galactosidase resulted in the formation of a deep blue product, and the proportion of positively stained deep blue cells was quantified.

#### ATP production measurement

ATP concentration was measured using the ATP Assay Kit (S0027, Beyotime, Shanghai, China). According to the manufacturer's instructions, primary FAPs from the Control group, Injury group, and Melatonin treatment group were lysed to obtain the supernatant for determining intracellular ATP levels. The detection solution was added to a 96-well plate and incubated at room temperature for 5 min. The supernatant was then added to the wells and mixed quickly. Finally, luminescence was measured using a microplate reader, and the total ATP concentration was calculated based on the luminescence signal.

#### Measurement of mitochondrial membrane potential

The mitochondrial membrane potential was assessed utilizing the Mitochondrial Membrane Potential Assay Kit with TMRE (C2001S, Beyotime, Shanghai, China). The TMRE working solution was prepared at a 1:1000 dilution. A total of  $3 \times 10^5$  primary FAPs from the Control, Injury, and Melatonin treatment groups were incubated at 37 °C for 30 min. Subsequently, the cells were washed with PBS and centrifuged at room temperature for 5 min to eliminate excess dye. The fluorescence intensity was then quantified using a flow cytometer.

#### Cell Immunofluorescence

Primary FAPs at a density of  $3 \times 10^4$  cells per group, derived from Control, Injury, and Melatonin-treated cohorts, were cultured on glass coverslips. Adhering to standard immunofluorescence protocols, the cells were fixed in 4% PFA for 15 min at room temperature, permeabilized with 0.1% Triton X-100 in PBS for 10 min, and subsequently blocked with 5% BSA for 30 min. After washing with PBS, the samples were incubated overnight at 4 °C with primary antibodies (MyHC: ab37484, Abcam, CA, USA). Following three washes with PBST, the cells were stained with an Alexa Fluor™ 488-conjugated secondary antibody (A-11001, Thermofisher, CA, USA) in 5% BSA at 37 °C for 1 h. Nuclei were counterstained using a DAPI-containing mounting medium (F6057, Sigma-Aldrich, MO, USA). Images were captured and visualized using a Zeiss 880 Laser Scanning Confocal Microscope equipped with Airyscan technology (ZEISS). Fluorescence quantification analysis was conducted utilizing ImageJ software.

#### Cell ROS assay

The intracellular levels of ROS were quantified using the CellRox™ Deep Red reagent (C10422, Thermofisher, CA, USA). Post-treatment, the cells underwent a PBS wash and were subsequently incubated with serum-free RPMI 1640 medium containing 5  $\mu$ M CellRox-red at 37 °C, protected from light, for a duration of 30 min. The stained cells were then subjected to analysis via flow cytometry using the Cytoflex LX system.

#### Western blot

For the western blot analysis, total protein was extracted from cell samples utilizing the radioimmunoprecipitation assay (RIPA) lysis buffer (P0013B, Beyotime, Shanghai, China). The protein concentration was quantified using a Bicinchoninic Acid (BCA) Protein Assay Kit (P0010, Beyotime, Shanghai, China). Proteins were subsequently separated via sodium dodecyl sulfate-polyacrylamide gel electrophoresis and transferred onto polyvinylidene fluoride membranes. The membranes were blocked with skimmed milk and incubated with the primary antibody overnight at 4 °C. Following this, incubation with the secondary antibody (ab205719/ab6721, Abcam, CA, USA) was conducted at room temperature for 1 h. Image acquisition was performed using the ChemiDoc™ Imaging System (Bio-Rad, Hercules, CA, USA). The main antibodies used in this study are as follows: p16: sc-1661, Santa Cruz, TX, USA; p21: sc-6246, Santa Cruz, TX, USA; p53: sc-99, Santa Cruz, TX, USA; pRB: 8516, cell signaling technology, MA, USA; RB: 9313, cell signaling technology, MA, USA;  $\alpha$ -tubulin: RM2003, ray-antibody, Beijing, China; Myosin: ab37484, Abcam, CA, USA; MyoD: sc-377,460, Santa Cruz, CA, USA; Myogenin: sc-12,732, Santa Cruz, CA, USA; Pax-7: sc-81,975, Santa Cruz, CA, USA; AMPK: ab32047, Abcam, CA, USA; p-AMPK: ab133448, Abcam, CA, USA; PGC1 $\alpha$ : ab191838, Abcam, CA, USA; LKB1: sc-374,300, Santa Cruz, CA, USA; GAPDH: ab9485, Abcam, CA, USA.

#### RNA isolation and real-time PCR

Primary FAPs from Control, Injury, and Melatonin-treated groups ( $1 \times 10^6$  cells per group) were lysed using TRIzol™ Reagent (1596018, Thermofisher, MA, USA) to facilitate total RNA extraction. Reverse transcription was conducted in accordance with the manufacturer's protocol utilizing the 5X All-In-One Master Mix (G485, Abm-Good, Richmond, Canada). The resultant complementary DNA (cDNA) templates were subsequently analyzed via quantitative real-time PCR (qRT-PCR) using the Power SYBR™ Green Master Mix (4367659, Thermofisher, MA, USA) on a QuantStudio™ 6 Flex Real-Time PCR System (Thermofisher, MA, USA). The primer sequences employed for qRT-PCR are provided in Table 1.

**Table 1** Primer sequences utilized in qRT-PCR

m-GAPDH	Forward:5'-GAAGGTGGTGAAGCAGGCATCT-3' Reverse:5'-CGGCATCGAAGGTGGAAGAGTG-3'
m-IL-1α	Forward:5'-GCACTTGGGAGCCCTTTCATCA-3' Reverse:5'-AGGACGGGAGGGAGAAAGACTG-3'
m-IL-6	Forward:5'-CTTGGGACTGATGCTGGTGACA-3' Reverse:5'-GCCTCCGACTTGTGAAGTGTA-3'
m-CXCL15	Forward:5'-CAGACGGACATGGCTGCTCAAG-3' Reverse:5'-GTGTACAGGGACGGACGAAGA-3'
m-MMP14	Forward:5'-CTGAGGAGGAGACGGAGGTGAT-3' Reverse:5'-GCCAGTACCAGGAGCAGAGTA-3'

**Table 2** Sequence of LKB1 siRNA

m-siNC	5'-UUCUCCGAACGUGUCACGUTT-3' 5'-ACGUGACACGUUCGGAGAATT-3'
m-siLKB1-1	5'-CAAGGCUGUUUGUGAAUUTT-3' 5'-AUUCACACAAACAGCCUUGTT-3'
m-siLKB1-2	5'-CAAUAUCUACAAGCUCUUUTT-3' 5'-AAAGAGCUUGUAGAUUUGTT-3'
m-siLKB1-3	5'-CCAAGCUCAUCGCAAGUATT-3' 5'-UACUUGCCGAUGAGCUUGGTT-3'

Cell co-culture

A Transwell co-culture system was employed using Millicell hanging cell culture chambers (0.4 μm pore size, polyethylene terephthalate, 24 wells; Millipore, Bedford, MA, USA). Each Millicell chamber was populated with approximately 3.5 × 10<sup>5</sup> FAPs derived from both normal and injured C57 mice. These chambers were positioned within a 24-well plate, with FAPs residing in the upper chamber and C2C12 cells, which were cultured on separate cell culture plates, located in the lower chamber, thereby establishing a co-culture system. The C2C12 cells were maintained in DMEM supplemented with 2% penicillin/streptomycin and 10% fetal bovine serum, serving as the growth medium.

Cell treatment and siRNA transfection

Primary FAP cells were categorized into three experimental groups: the **injury** group, **injury + Mel** group, and **injury + compound** group. FAPs were treated with melatonin at a final concentration of 10 μM for a duration of five days, and with compound C (S7840, Selleck Chemicals, Houston, TX, USA) at a final concentration of 4 μM for 24 h, as referenced in studies ([34, 35]. The cells were cultured to achieve 60–80% confluence using an appropriate culture medium, ensuring that they remained healthy and in an actively proliferating state. Small interfering RNA (siRNA) was designed to target the gene of interest, as detailed in Table 2. The transfection reagent Lipo3000 (L3000075, Thermofisher, MA, USA) was prepared in accordance with the manufacturer's instructions. The siRNA was combined with the transfection reagent and added to a serum-free medium, allowing it to incubate for 10 min. The siRNA-transfection reagent

complex was then introduced to the cells, followed by gentle swirling of the culture dish, and the cells were incubated in a 37 °C CO<sub>2</sub> incubator. After 48 h, the cells were harvested, and protein extraction was performed to facilitate subsequent experimental procedures.

Statistical analysis

The experimental results are presented as the mean ± standard error of the mean. Statistical analyses were conducted utilizing GraphPad Prism 8 software, and unpaired Student's t-test or one-way ANOVA was used for statistical analysis. A p-value of less than 0.05 was deemed statistically significant. The significance levels of the p-values are denoted as follows: \**p* < 0.05, \*\**p* < 0.01, \*\*\**p* ≤ 0.001, and NS indicates not significant (*p* ≥ 0.05) ([36].

Results

FAPs exhibited a senescent phenotype following acute skeletal muscle injury

To analyze changes in muscle cell populations after skeletal muscle injury, we downloaded scRNA-seq data on skeletal muscle injury from the Gene Expression Omnibus (GEO) database with accession number GSE214892. We performed high-throughput, droplet-based scRNA-seq to analyze the transcriptomes of individual mononuclear cells prepared from tibialis anterior (TA) muscles were collected from C57BL/6 mice 5 days between control groups (50μL PBS injection) and injury groups (50μL 10μM CTX injection). Unsupervised cell clustering analysis identified 8 distinct cell groups, including Satellite Cells, Endothelial Cells, Myonuclei, Immune, FAPs, Mural, Tendon, and Schwann (Fig. 1A, S1A-D). Cell type-specific markers were used to differentiate and identify these cell populations (Fig. 1B). Single-cell data analysis revealed that cells with a high senescence score were more concentrated in the FAPs population (Fig. 1C). Further analysis showed that the senescence score of FAPs increased after injury (Fig. 1D). GO and KEGG pathway analyses indicated that these DEGs were enriched in aging-related signaling pathways: p53 signaling pathway and oxidative stress regulation pathway (Fig. 1E). Notably, compared to the control group, 12 aging-related genes, including Cdkn1a, Foxo3, Hipk3, Gadd45b, and Fas, exhibited higher expression in the injury group (Fig. 1F). To substantiate our findings further, we referenced another single-cell dataset (GSE138826) for bioinformatics analysis (Figure S2-3). Our analysis also revealed that cells exhibiting elevated senescence scores were predominantly concentrated within the FAPs population (Figure S2A-C). Further analysis demonstrated an increase in the senescence score of FAPs following injury (Figure S2D). GO and KEGG pathway analyses indicated that these DEGs were enriched in oxidative

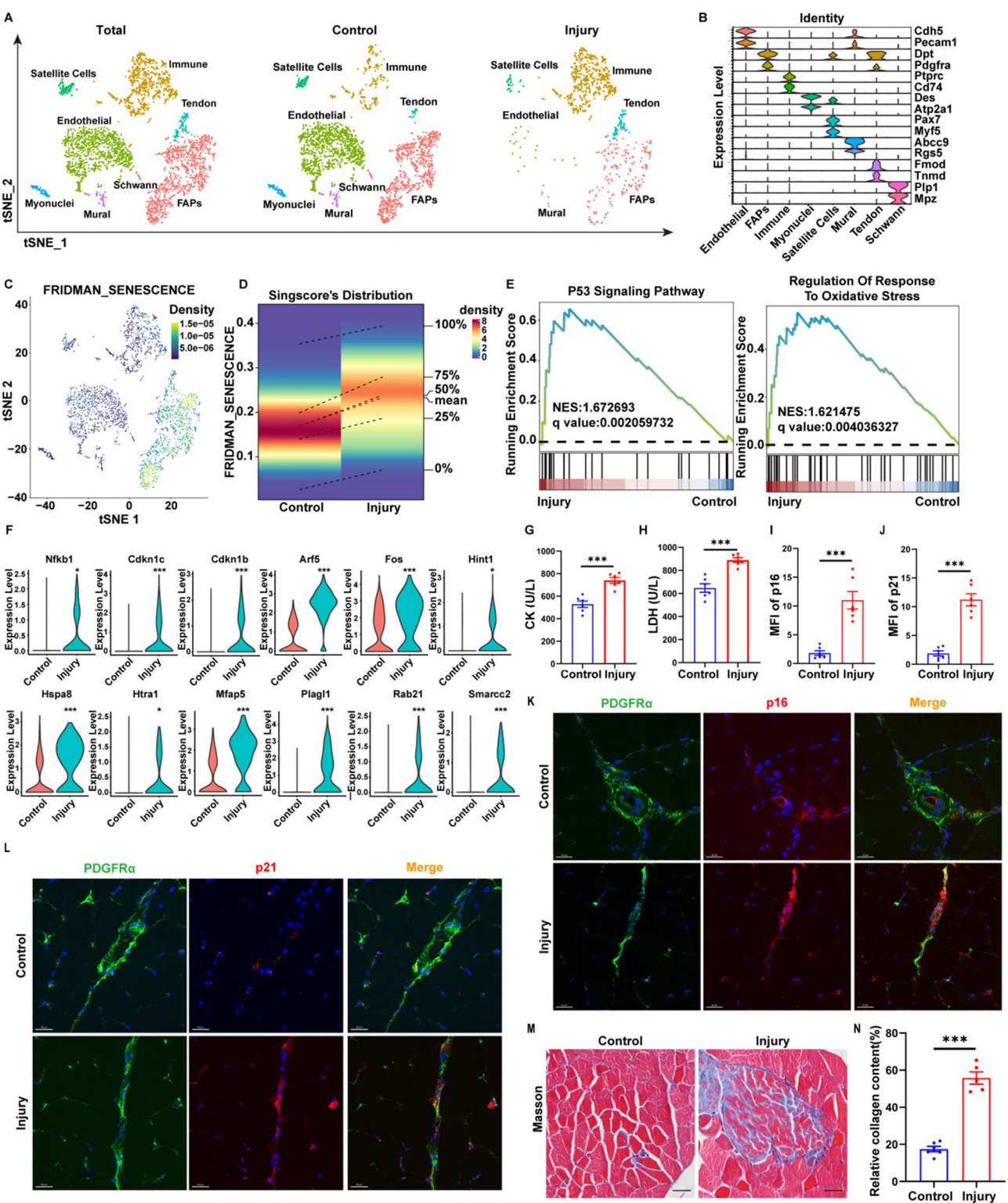


**Fig. 1** (See legend on next page.)



(See figure on previous page.)

**Fig. 1** FAPs exhibited a senescence phenotype following acute skeletal muscle injury. **A:** Cell clusters of the sc-RNA-seq data from database GSE214892 (GEO Accession viewer (nih.gov)). Tibialis anterior muscle were collected from C57BL/6 mice 5 days between control groups (50  $\mu$ L PBS injection) and injury groups (50  $\mu$ L 10  $\mu$ M CTX injection) ( $n=5$  mice for each group). **B:** The bubble plot showed the expression of distinctive marker genes in eight cell types. The dot size indicates the percentage of gene expression, and the dot color indicates the average expression level. **C:** The tSNE plot of different cell subtypes in (A) **D:** Density profiles of senescent fractions in (A) **E:** GSEA analysis of the p53 pathway and the oxidative stress pathway in (A) **F:** Violin plot of senescence-related genes for FAPs in (A). **G-H:** The level of serum CK(G), LDH(H) from C57BL/6 mice 3 days between control (50  $\mu$ L PBS injection) and injury groups (50  $\mu$ L 10  $\mu$ M CTX injection) ( $n=6$  mice for each group). **I-J:** The Relative MFI of p16(I) and p21(J) in tibialis anterior muscle. **K-L:** Representative immunofluorescence images of the senescent FAPs (PDGFR $\alpha$  positive and p16/p21 positive cells) in tibialis anterior muscle. Scale bar = 20  $\mu$ m. **M-N:** Masson trichrome staining (mice,  $n=6$ ) and quantification analysis of muscle fibrosis level in tibialis anterior muscle. Scale bar = 25  $\mu$ m. The data above are presented as mean  $\pm$  SEM of three independent experiments, P-values are calculated between two groups was performed using an unpaired t-test (ns, not significant; \* $P < 0.05$ ; \*\* $P < 0.01$ ; \*\*\* $P < 0.001$ .)

stress regulation pathway (Figure S2E). Therefore, we conducted the muscle injury model by injecting CTX (50  $\mu$ L, 10  $\mu$ M), and verified its successful establishment by measuring CK and LDH levels (Fig. 1G-H). To further illustrate senescence of FAPs during injury, we performed muscle section staining and found an increase in the MFI of p16 or p21 in FAPs after CTX injury (Fig. 1I-L). Literature reports suggested that the senescent FAPs might differentiate into adipocytes or myofibroblasts, contributing to ectopic fat deposition and fibrosis in skeletal muscle ([37]. Therefore, we analyzed muscle fibrosis post-injury using Masson trichrome staining. Results showed an increase in muscle fibrosis after injury (Fig. 1K-M). These findings suggested that FAPs underwent senescence after injury.

#### In vitro validation of acute skeletal muscle injury-induced FAP senescence and redox imbalance

To further verify the senescence of FAPs after injury, we isolated CD31<sup>-</sup> CD45<sup>-</sup> PDGFR $\alpha$ <sup>+</sup> Sca-1<sup>+</sup> cells, identified as FAPs (Fig. 2A), following previously reported methods ([38]. Interestingly, we found the amount of FAPs decreased after CTX injury, suggesting that the function and feature of FAPs changed after injury (Fig. 2B). SA- $\beta$ -Gal analysis revealed a significant increase in SA- $\beta$ -Gal-positive cells in the FAPs of the injury group (Fig. 2C-D), suggesting that CTX-induced skeletal muscle injury promoted FAP senescence. Western blot analysis showed significantly elevated levels of the cell cycle-related proteins p16, p21, and p53, while pRB levels were significantly decreased in injury group of FAPs compared to control group (Fig. 2E-F). To investigate the cause of senescence in FAPs, we further assessed the level of oxidative stress in FAPs within each group and found that the levels of ROS was markedly increased in the injury group of FAPs (Fig. 2G-H). The mitochondria are the main cellular organelles responsible for clearing ROS within the cell ([39]. We assessed the mitochondrial membrane potential and ATP production capacity in FAPs using TMRE staining and ATP detection. The results indicated the diminished mitochondrial function post-injury, characterized by decreased membrane potential and ATP production (Fig. 2I-K). Additionally, mRNA levels of IL-1 $\alpha$ ,

IL-6, CXCL-15, and MMP14 (factors secreted by senescent cells) were significantly increased of FAPs sorted in injury group FAPs (Fig. 2L). The above study showed that FAPs exhibited a senescent phenotype during post-injury. However, the relationship between FAP senescence and the regeneration of skeletal muscle remains unclear.

#### Melatonin maintained redox homeostasis and alleviated FAP senescence

In the above studies, we found that the FAP senescence involves redox homeostasis imbalance, mitochondrial dysfunction, and increased reactive oxygen species (ROS) levels. Therefore, we wonder whether the senescence of FAPs can be inhibited by anti-oxidants. Melatonin (Mel), the indoleamine hormone synthesized and secreted by the pineal gland, protects stem cells by eliminating free radicals, upregulating the expression of antioxidant enzymes, reducing the activity of prooxidant enzymes, and maintaining mitochondrial homeostasis ([40]. After adding melatonin to the in vitro culture environment (Fig. 3A), we found a significant decrease in SA- $\beta$ -Gal-positive cells (Fig. 3B-C). Furthermore, we assessed the impact of melatonin on FAPs senescence through Western blot, revealing that cellular senescence was alleviated following melatonin treatment (Fig. 3D-E). Subsequently, measuring intracellular ATP levels revealed that melatonin restored ATP production capacity in injury group FAPs (Fig. 3F). Additionally, we analyzed changes in cellular ROS levels and mitochondrial membrane potential using flow cytometry, indicating that melatonin promotes the restoration of mitochondrial function in injury group FAPs, manifesting as increased ROS clearance and membrane potential recovery (Fig. 3G-J). These findings demonstrated that in vitro melatonin treatment effectively mitigated the senescence of FAPs induced by injury.

#### FAP senescence diminished their capacity to promote the differentiation of C2C12

Research indicates that the primary function of FAPs is associated with paracrine mechanisms, secreting a range of cytokines (including IGF-1, IL-6, Wnt1, Wnt3A, and Wnt5A) to promote the differentiation of muscle stem



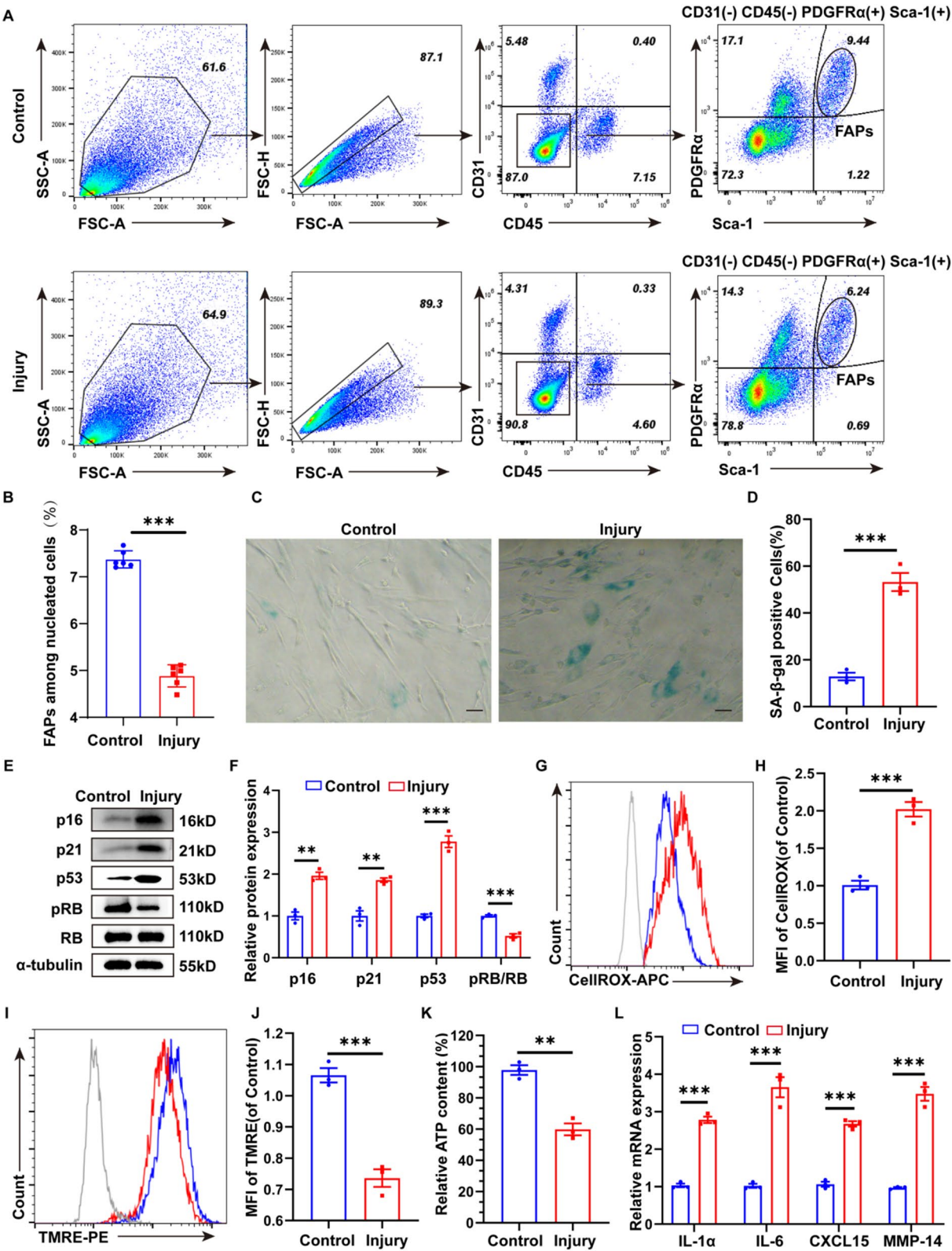


Fig. 2 (See legend on next page.)

(See figure on previous page.)

**Fig. 2** In vitro validation of acute skeletal muscle injury-induced FAP senescence and redox imbalance. **A:** Flow cytometry sort the FAPs (CD31<sup>−</sup> CD45<sup>−</sup> PDGFR $\alpha$ <sup>+</sup> Sca-1<sup>+</sup> cells) from tibialis anterior muscle which were collected from C57BL/6 mice 3 days between control groups (50  $\mu$ L PBS injection) and injury groups (50  $\mu$ L 10  $\mu$ M CTX injection) ( $n=6$  mice for each group). **B:** The percentage of FAPs among nucleated cells in (A). **C–D:** SA- $\beta$ -Gal images ( $n=3$ ) and quantification analysis showed the number of SA- $\beta$ -Gal-positive cells in (A). Scale bar: 50  $\mu$ m. **E–F:** Western Blot analysis ( $n=3$ ) of the proteins associated with cell senescence (p16, p21, p53, p-RB and RB) in (A). **G–H:** Flow cytometry and quantification analyses of CellROX fluorescence ( $n=3$ ) indicated the level of ROS in (A). **I–J:** Flow cytometry and quantification analyses of TMRE fluorescence ( $n=3$ ) indicated the level of mitochondrial membrane potential in (A). **K:** Quantification analyses of ATP content ( $n=3$ ) of (A). **L:** qRT-PCR analysis of the SASP genes (IL-1 $\alpha$ , IL-6, CXCL15 and MMP-14) in (A). The data above are presented as mean  $\pm$  SEM of three independent experiments, P-values are calculated between two groups was performed using an unpaired t-test (ns, not significant; \* $P < 0.05$ ; \*\* $P < 0.01$ ; \*\*\* $P < 0.001$ .)

cells. To further explore the role of FAP senescence in the skeletal muscle regeneration, we co-cultured FAPs from different groups with muscle stem cells C2C12 (Fig. 4A). MyHC is an index of myogenic differentiation of C2C12. Immunofluorescence staining for MyHC revealed a significant reduction in the ability of injury group FAPs to promote C2C12 differentiation, which was alleviated by melatonin treatment (Fig. 4B–C). Western blot analysis showed that melatonin restored the expression of differentiation markers Myosin, MyoD, Myogenin, and Pax-7 in C2C12 cells from the injury group (Fig. 4D–E). These findings indicated that post-injury senescence of FAPs diminished their ability to promote MuSC differentiation and melatonin can mitigate this impairment, but the precise mechanism remains unclear.

#### Melatonin alleviated FAP senescence via AMPK activation

To explore the mechanism by which melatonin alleviated FAP senescence, we analyzed RNA-seq data (GSE214008) from melatonin-treated FAPs. We found that melatonin treatment led to downregulation of 1253 genes and upregulation of 443 genes, with the AMPK signaling pathway notably enriched (Fig. 5A–B, S4A). AMPK, a key energy-sensing enzyme, regulates cellular metabolism and oxidative defense ([41]. Next, we examined the change of protein expression level of AMPK signaling pathway of FAPs after Melatonin treatment. The results showed that the AMPK signaling pathway was activated in FAPs after melatonin treatment. (Fig. 5C–D). Meanwhile, we tested this further using Compound C, an AMPK inhibitor.  $\beta$ -Gal staining showed an increase in  $\beta$ -gal-positive cells with Compound C treatment (Fig. 5E–F). Flow cytometry revealed that Compound C impaired mitochondrial function in FAPs, increasing ROS levels and decreasing membrane potential (Fig. 5G–J). Besides, we used siRNA transfection technique to knock down LKB1, a key regulatory factor of AMPK pathway, in FAPs (Figure S5A–B). Then we tested the change of the aging related gene expression in FAPs after siRNA transfection. The results showed that the effect of melatonin to delay senescence of FAPs reduced after knocking down the LKB1 (Fig. 5K–L). These results suggested that the effects of melatonin effects on alleviating FAP senescence are mediated through AMPK signaling pathway activation.

#### Antioxidant intervention in FAPs restored muscle function

To verify melatonin's role in promoting muscle repair in vivo, we established a melatonin treatment model by administering intraperitoneal injections of melatonin following acute muscle injury induced by CTX. After 15 days of treatment, muscle samples were collected (Fig. 6A). Immunofluorescence staining showed a decrease in PDGFR $\alpha$ <sup>+</sup>p16<sup>+</sup> and PDGFR $\alpha$ <sup>+</sup>p21<sup>+</sup> cells, indicating reduced FAP senescence with melatonin treatment (Fig. 6B–D, S6A–B). Histological assessments with Sirius Red, Masson Trichrome and glycogen PAS staining revealed reduced fibrosis, improved muscle glycogen content and storage capacity post-injury with melatonin treatment (Fig. 6E–I). These results demonstrated that melatonin treatment alleviated FAP senescence, aiding muscle repair and restoring muscle function.

In summary, our study found that oxidative-reduction homeostasis imbalance and cellular senescence occurred in FAPs following acute injury, leading to a decline in skeletal muscle regeneration and repair functions. However, melatonin treatment alleviated the senescence of FAPs, thereby promoting the recovery of muscle repair functions. These results suggested that melatonin had potential as an intervention to improve muscle repair capacity impaired by FAP senescence.

#### Discussion

In this study, we utilized single-cell data to discover that FAPs exhibited a senescent phenotype during acute skeletal muscle injury. We employed the anti-oxidant small molecule drug melatonin to mitigate the senescence of FAPs and restore their regenerative and repair capabilities in skeletal muscle.

Interestingly, we found the amount of FAPs decreased after CTX injury. On one hand, it may be due to the senescence and apoptosis of the FAPs; On the other hand, the alteration in the inflammatory microenvironment during muscle injury may lead to an increase in immune cells, which then phagocytize FAPs, thereby reducing their numbers.

Recent studies have indicated that FAPs play a dual role in muscle regeneration ([13, 42, 43]. On one hand, they maintain the renewal of muscle stem cells and facilitate tissue repair. On the other hand, they may also contribute to the formation of fibrosis scars and ectopic

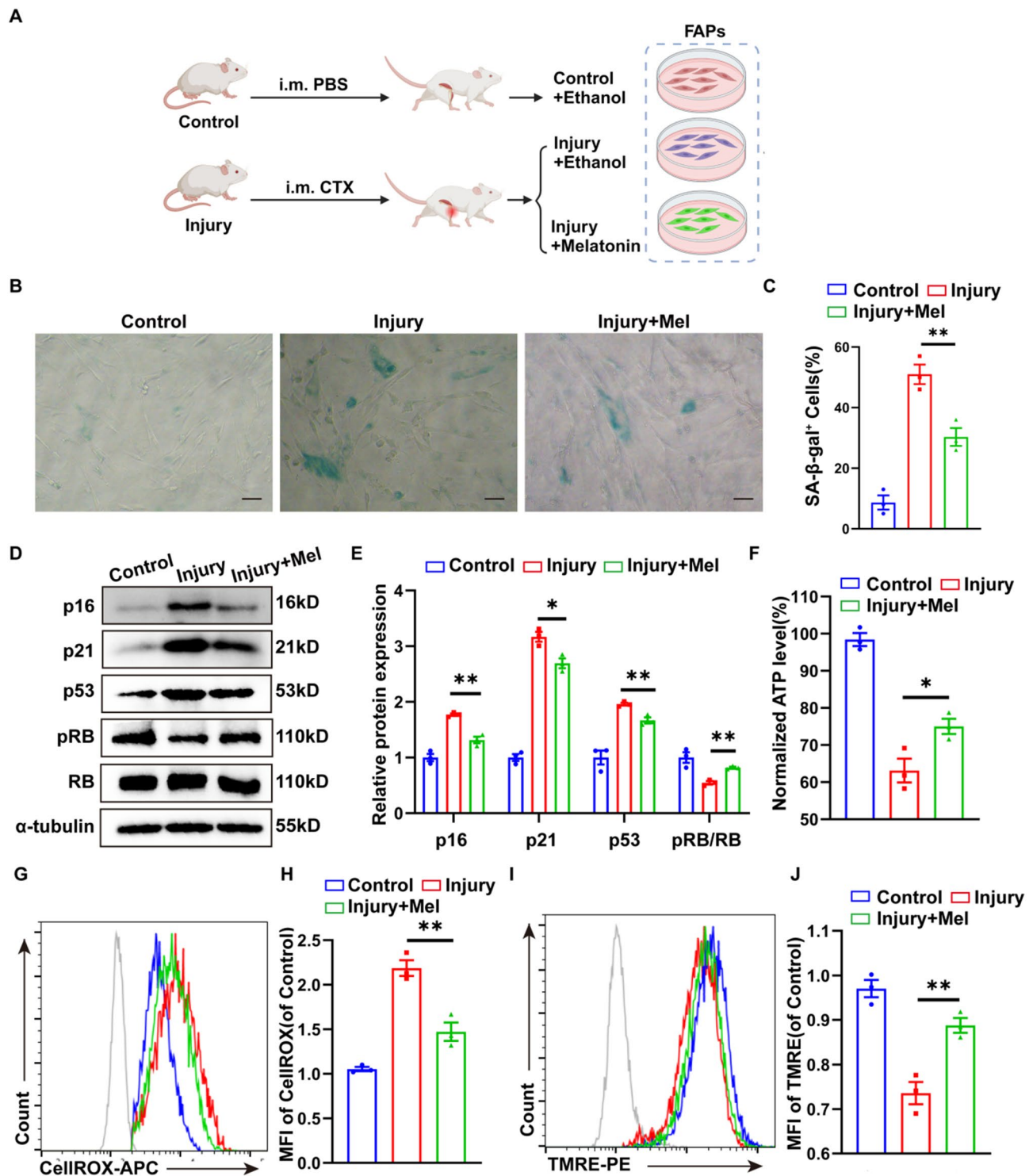


**Fig. 3** Melatonin maintained redox homeostasis and alleviated FAP senescence. **A:** Schematic diagram of FAPs in vitro experiment. Flow cytometry sort FAPs from tibialis anterior muscle which were collected from C57BL/6 mice 3 days between control groups (50μL PBS injection) and injury groups (50μL 10μM CTX injection), then the FAPs of Control and the Injury group were treated with ethanol (vehicle, 5 days) and the FAPs of Injury + Mel groups were treated with melatonin (100μM, 5 days). **B-C:** SA-β-Gal images ( $n=3$ ) and quantification analysis showed the number of SA-β-Gal-positive cells in FAPs of (A). Scale bar: 50 μm. **D-E:** Western Blot analysis ( $n=3$ ) of the proteins associated with cell senescence (p16, p21, p53, p-RB and RB) in FAPs of (A). **F:** Quantification analyses of ATP content ( $n=3$ ) of FAPs in (A). **G-H:** Flow cytometry and quantification analyses of CellROX fluorescence ( $n=3$ ) indicated the levels of ROS in FAPs of (A). **I-J:** Flow cytometry and quantification analyses of TMRE fluorescence ( $n=3$ ) indicated the levels of mitochondrial membrane potential in FAPs of (A). The data above are presented as mean  $\pm$  SEM of three independent experiments, P-values were calculated between three groups were performed using one-way analysis of variance (anova) followed by the Tukey multiple-comparison test. (ns, not significant; \* $P < 0.05$ ; \*\* $P < 0.01$ ; \*\*\* $p < 0.001$ .)

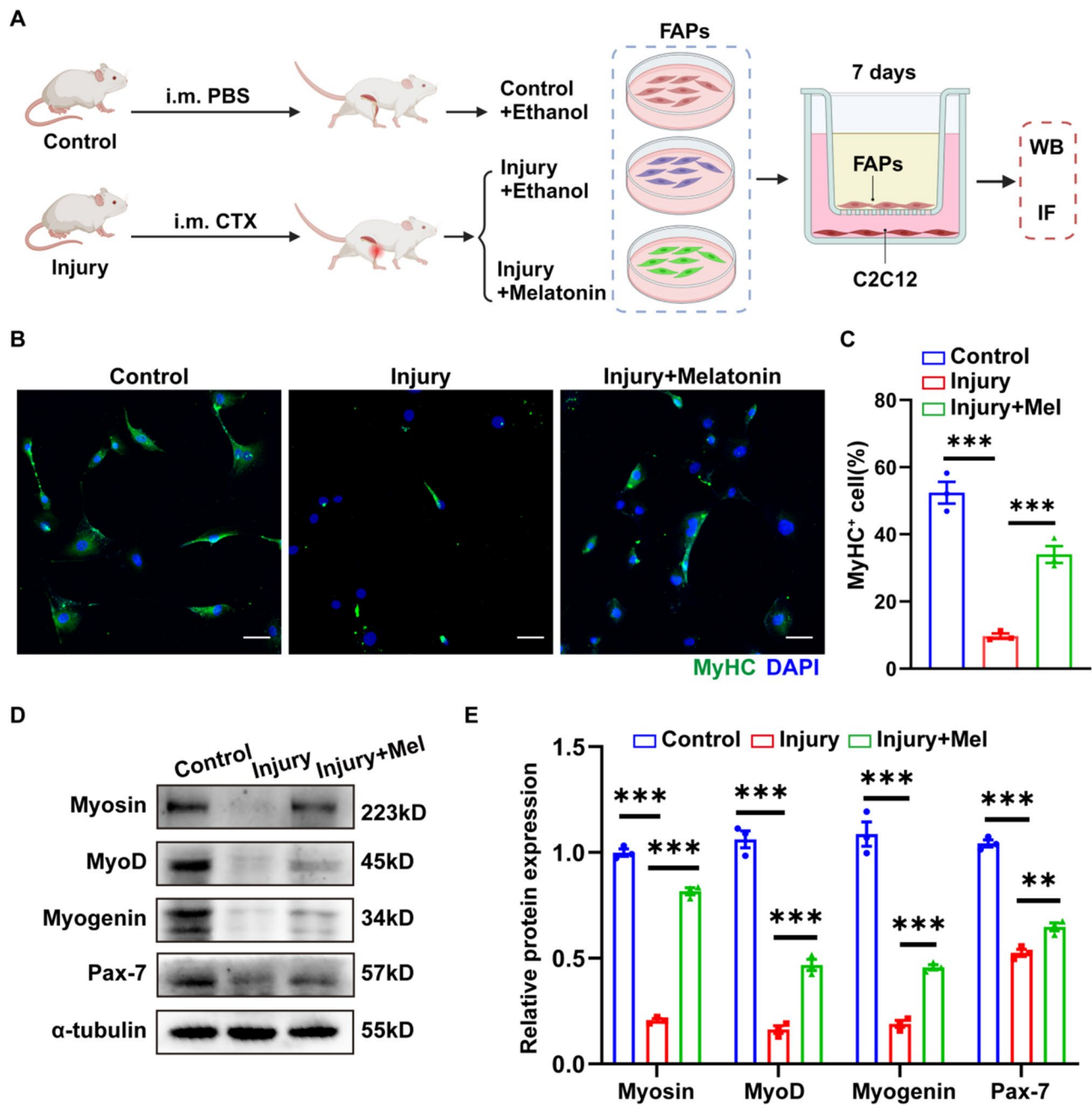


**Fig. 4** FAP senescence diminished their capacity to promote the differentiation of C2C12. **A:** Schematic diagram of FAPs-C2C12 coculture system. Flow cytometry sorted FAPs from tibialis anterior muscle which were collected from C57BL/6 mice 3 days between control groups (50μL PBS injection) and injury groups (50μL 10μM CTX injection), then the FAPs of Control and the Injury group were treated with ethanol (vehicle, 5 days) and the FAPs of Injury+Mel groups were treated with melatonin (100μM, 5 days). FAPs were cultured in top compartment and the C2C12 were cultured in the bottom. The FAPs and C2C12 were coculture for 7days. Indicators of differentiation were analyzed by WB and IF. Created with BioRender.com. **B-C:** Representative immunofluorescence images and quantification analyses displayed the differentiated C2C12 in (A). Scale bar = 50 μm. **D-E:** Western Blot analysis ( $n=3$ ) of the proteins associated with differentiation degree (Myosin, MyoD, Myogenin and Pax-7) in C2C12 in (A). The data above are presented as mean  $\pm$  SEM of three independent experiments, P-values are calculated between three groups were performed using one-way analysis of variance (anova) followed by the Tukey multiple-comparison test. (ns, not significant; \* $P < 0.05$ ; \*\* $P < 0.01$ ; \*\*\* $p < 0.001$ .)



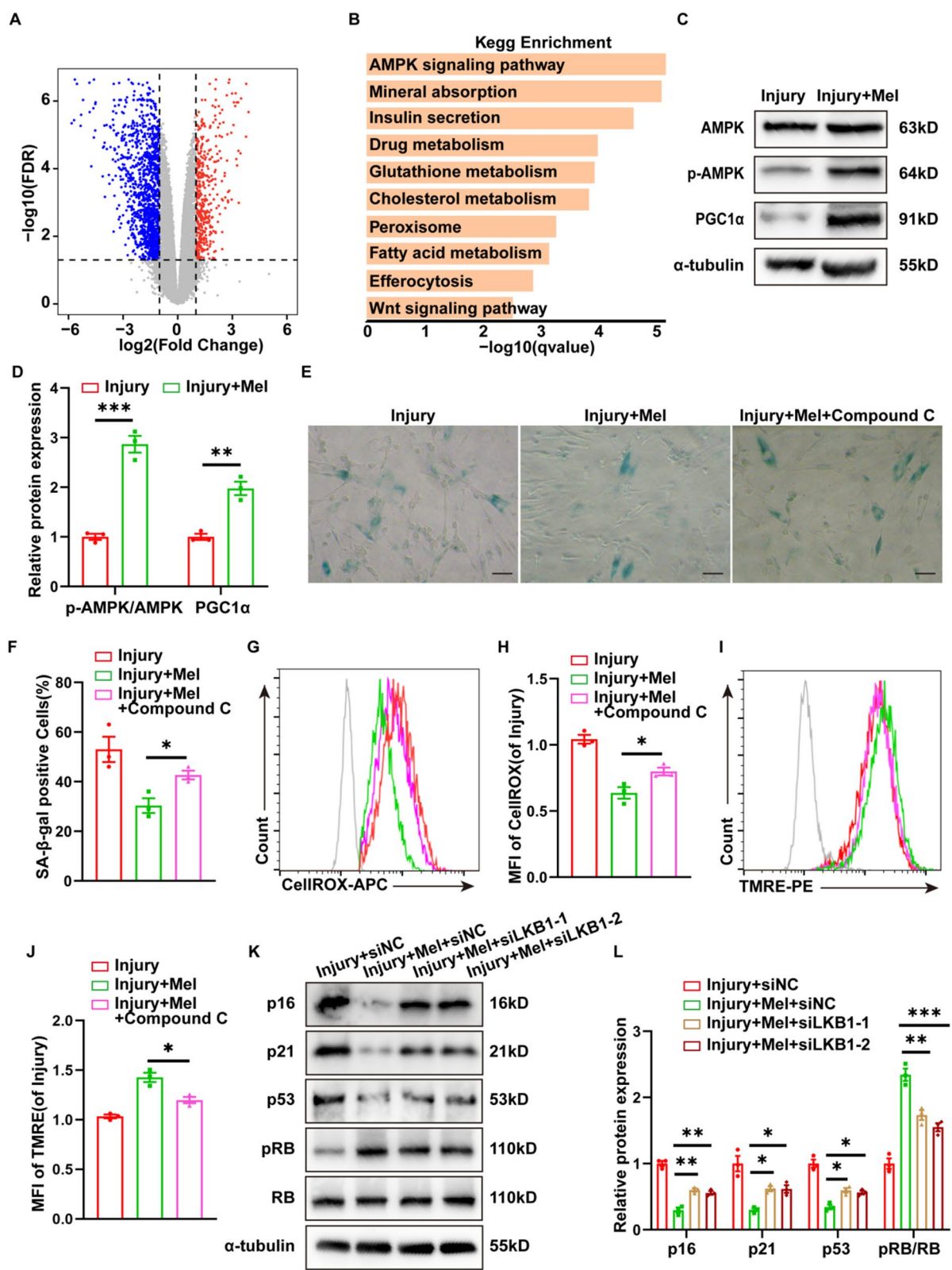


Fig. 5 (See legend on next page.)

(See figure on previous page.)

**Fig. 5** Melatonin acts via AMPK activation. **A-B:** GO and KEGG pathway analyses of FAPs from database GSE214008. FAPs were sorted from tibialis anterior muscle which were collected from C57BL/6 mice and treated with vehicle or melatonin for 24 h in vitro. **C-D:** Western Blot analysis of the proteins ( $n=3$ ) associated with AMPK signal pathway (p-AMPK, AMPK, PGC1 $\alpha$ ) in FAPs from tibialis anterior muscle which were collected from C57BL/6 mice 3 days after CTX(50 $\mu$ L, 10 $\mu$ M) injection, then the FAPs of Injury group were treated with ethanol (vehicle, 5 days) and the FAPs of Injury + Mel groups were treated with melatonin(100 $\mu$ M, 5 days). **E-F:** SA- $\beta$ -Gal images( $n=3$ ) and quantification analysis showed the number of SA- $\beta$ -Gal-positive cells in FAPs from tibialis anterior muscle which were collected from C57BL/6 mice 3 days after CTX(50 $\mu$ L, 10 $\mu$ M) injection, then the FAPs of Injury group were treated with ethanol (vehicle, 5 days), the FAPs of Injury + Mel groups were treated with melatonin(100 $\mu$ M, 5 days) and the FAPs of Injury + Mel + Compound C groups were treated with melatonin(100 $\mu$ M, 5 days) and compound C (4  $\mu$ M, 24 h). **G-H:** Flow cytometry and quantification analyses of CellROX fluorescence( $n=3$ ) indicated the level of ROS in FAPs in Injury, Injury + Mel, Injury + Mel + Compound C groups. **I-J:** Flow cytometry and quantification analyses of TMRE fluorescence( $n=3$ ) indicated the level of mitochondrial membrane potential in FAPs in Injury, Injury + Mel, Injury + Mel + Compound C groups. **K-L:** Western Blot analysis of the proteins associated with cell senescence (p16, p21, p53, p-RB and RB) in FAPs from tibialis anterior muscle which were collected from C57BL/6 mice 3 days after CTX(50 $\mu$ L, 10 $\mu$ M) injection, then the FAPs were transfected with siNC or siLKB1-1 or siLKB1-2. The FAPs of Injury + siNC groups were treated with ethanol (vehicle, 5 days), and the FAPs of groups among Injury + Mel + siNC, Injury + Mel + siLKB1-1, Injury + Mel + siLKB1-2 were treated with melatonin (100 $\mu$ M, 5 days). The data above are presented as mean  $\pm$  SEM of three independent experiments, P-values are calculated between two groups was performed using an unpaired t-test, and multiple-group statistical analysis was performed using one-way analysis of variance (anova) followed by the Tukey multiple-comparison test. (ns, not significant; \* $P<0.05$ ; \*\* $P<0.01$ ; \*\*\* $P<0.001$ .)

fat infiltration, thereby compromising the integrity and function of skeletal muscle tissue. Recent researches have primarily focused on the abnormal activation and differentiation of FAPs into fat cells or myoblasts in chronic skeletal muscle injury, leading to the formation of fat and fibers and participating in ectopic fat deposition and fibrosis of skeletal muscle ([44]. However, our study revealed that FAPs become senescent during acute skeletal muscle injury, resulting in a decline in the regenerative and repair functions of skeletal muscle.

Cellular senescence is a complex biological process primarily caused by DNA damage and telomere shortening, epigenetic changes such as alterations in DNA methylation patterns and abnormal histone modifications, organelle dysfunction, extracellular matrix changes, intercellular signaling disruptions, and oxidative stress ([45]. Senescent cells typically exhibit an inflammatory response and secrete senescence-associated secretory phenotype (SASP) factors that alter the surrounding cellular environment, promoting tissue senescence and pathological changes ([46]. The senescence of muscle is closely associated with an increase in cellular senescence, a state of irreversible cell cycle arrest ([47]. Studies have shown that during muscle aging, the number and proliferative capacity of FAPs decline, while the trend of fibrotic differentiation increases ([8, 48]. Moreover, changes in FAPs phenotype may be mediated by changes in the microenvironment during muscle senescence ([49, 50]. Therefore, further research is needed to explore the causes of FAP senescence and their role in the pathogenic mechanisms of skeletal muscle injury repair dysfunction.

Our experimental results indicated that oxidative-reduction homeostasis imbalance was a key factor leading to the senescence and functional impairment of FAPs. Following skeletal muscle injury, increased ROS and their accumulation beyond the cell's antioxidant capacity result in oxidative stress, causing damage to cellular structure and function, thus promoting

the senescence of FAPs. Therefore, alleviating oxidative stress in FAPs triggered by injury represents a novel therapeutic approach for treating skeletal muscle injury. Melatonin, an indoleamine hormone synthesized and secreted by the pineal gland, is well-known for its antioxidant properties ([51]. It has been reported that melatonin protects stem cells by scavenging free radicals, enhancing the expression of antioxidant enzymes, reducing the activity of pro-oxidant enzymes, and maintaining mitochondrial homeostasis ([52–54]. Additionally, melatonin, a commonly used health supplement, is widely employed to enhance sleep quality and regulate circadian rhythms. Data from animal and human studies show that low-dose melatonin use is relatively safe, while long-term or high-dose use might cause some adverse effects like dizziness, drowsiness, and nausea ([55]. Our study indicated that melatonin treatment alleviated the senescence of FAPs and enhanced mitochondrial function. Further bioinformatics analysis and in vitro experiments revealed that melatonin exerted its effects by activating the AMPK pathway. AMPK, a crucial enzyme for cellular energy sensing, is involved in regulating cellular metabolism and antioxidant defense ([56–58]. By activating the AMPK pathway, melatonin reduced ROS production, alleviates the senescence of FAPs, and maintains their normal functional state.

In this study, we investigated the changes in FAPs following acute skeletal muscle injury and the role of melatonin in treating skeletal muscle injury, achieving promising results. Currently, there are no significantly effective clinical treatments for muscle injuries, often relying on lifestyle changes and postoperative rehabilitation. Therefore, these findings provide evidence that antioxidant small molecules can alleviate the senescence of FAPs and improve their regenerative repair capability. Further research into FAPs function may enable more refined treatments based on disease models, which can be explored in future studies.

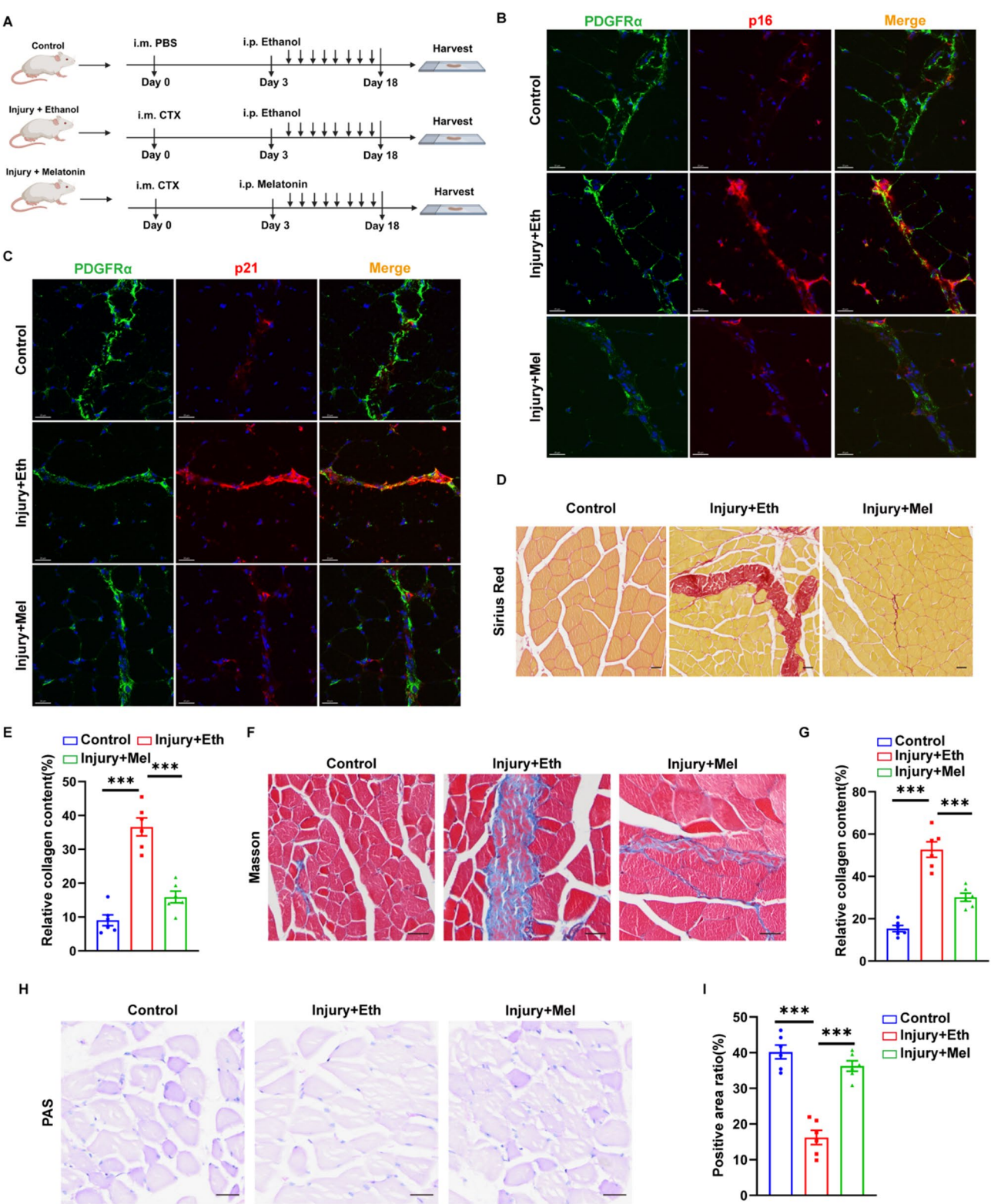


**Fig. 6** (See legend on next page.)



(See figure on previous page.)

**Fig. 6** Antioxidant intervention in FAPs restored muscle function. **A:** Diagram of in vivo experimental modalities for melatonin treatment of skeletal muscle injury. The PBS (50μL) and CTX (50μL, 10μM) were injected into the tibialis anterior muscle of C57BL/6 mice for 3 days. Then the Control and Injury+Eth groups were injected intraperitoneally of Ethanol lasting for 15 days and the Injury+Mel groups were injected intraperitoneally of 20 mg/kg/day melatonin lasting for 15 days. Created with BioRender.com. **B-C:** Representative immunofluorescence (mice,  $n=6$ ) images displayed the senescent FAPs (PDGFRα positive and p16/p21 positive cells) among Control, Injury and Injury+Mel group. Scale bar = 20 μm. **D-G:** Sirius Red (mice,  $n=6$ ) and Masson staining (mice,  $n=6$ ) and quantification analysis indicated the muscle fibrosis level among Control, Injury and Injury+Mel group. Scale bar: 25 μm. **H-I:** PAS staining (mice,  $n=6$ ) and quantification analysis indicated the muscle glycogen reserve capacity among Control, Injury and Injury+Mel group. The data above are presented as mean ± SEM of three independent experiments, P-values are calculated between two groups was performed using an unpaired t-test, and multiple-group statistical analysis was performed using one-way analysis of variance (anova) followed by the Tukey multiple-comparison test. (ns, not significant; \* $P < 0.05$ ; \*\* $P < 0.01$ ; \*\*\* $p < 0.001$ .)

## Conclusion

In this study, we first found FAPs underwent senescence and redox homeostasis imbalance after injury. Next, we utilized melatonin to enhance FAP regenerative and repair capabilities by activating AMPK signaling pathway. Taken together, this work provides a novel theoretical foundation for treating skeletal muscle injury.

## Abbreviations

MuSCs	Muscle Stem Cells
FAPs	Fibro-Adipogenic Progenitor Cells
PBS	Phosphate Buffered Saline
BSA	Bovine Serum Albumin
DMEM	Dulbecco's modified Eagle's medium
FBS	Fetal Bovine Serum
CTX	Cardiotoxin
TA	Tibialis Anterior muscle
GO	Gene Ontology
KEGG	Kyoto Encyclopedia of Genes and Genomes
TMRE	Tetramethylrhodamineethyl ester perchlorate
ROS	Reactive Oxygen Species

## Supplementary Information

The online version contains supplementary material available at <https://doi.org/10.1186/s13287-025-04242-4>.

Supplementary Material 1

Supplementary Material 2

## Acknowledgements

The authors gratefully thank the core research facilities from Shenzhen Campus of Sun Yat-sen University. The graphical abstract was created with BioRender.com. The authors declare that they have not used Artificial Intelligence in this study.

## Author contributions

Yuqing Yao conducted the experiments, arranged the figures, and authored the initial draft. Yusheng Luo performed the bioinformatic analysis. Xiaomei Liang, Li Zhong, Zhengchao Hong and Chao Song performed in vivo and in vitro experiments. Yannan Wang, Zeyu Xu performed data analysis. Jiancheng Wang and Miao Zhang revised the manuscript. All authors read and approved the final manuscript.

## Funding

The funding for this project was provided by the National Natural Science Foundation of China (32170799), Guangdong Basic and Applied Basic Research Foundation (2023B1515020016), Research Start-up Fund of the Seventh Affiliated Hospital, Sun Yat-sen University (393011), Fundamental Research Funds for the Central Universities, Sun Yat-sen University (23ykj003), Shenzhen Medical Research Fund (A2402005, 00201314003), Research Project on Science and Technology Innovation and Sports Culture Development of Guangdong Provincial Sports Bureau (GDSS2024NO24).

## Data availability

The data supporting the findings of this study can be obtained from the corresponding author upon reasonable request.

## Declarations

### Ethics approval and consent to participate

All animal experiments were performed in accordance with approved protocols by the Institutional Animal Care and Use Committee (IACUC) of Shenzhen LingFu TopBiotech. Co., LTD. and were reported in line with the ARRIVE guidelines 2.0. (1) Title of the approved project: The Role of Oxidative Stress-Mediated Fibro-Adipogenic Progenitors Senescence in Skeletal Muscle Regeneration and Repair; (2) Name of the institutional approval committee: IACUC of Shenzhen LingFu TopBiotech. Co., LTD.; (3) Approval number: TOPGM-IACUC-2023-0200; (4) Date of approval: November 11th, 2023.

### Consent for publication

All authors have confirmed their consent for publication.

### Conflict of interest

The authors assert that they do not have any conflicts of interest.

### Author details

<sup>1</sup>Scientific Research Center, The Seventh Affiliated Hospital of Sun Yat-sen University, Shenzhen, Guangdong 518107, China

<sup>2</sup>Department of Physical Education, Sun Yat-sen University, Guangzhou, China

<sup>3</sup>Guangdong Provincial Key Laboratory of Digestive Cancer Research, The Seventh Affiliated Hospital of Sun Yat-sen University, Shenzhen, China

<sup>4</sup>Department of Hematology, The Seventh Affiliated Hospital of Sun Yat-sen University, Shenzhen, China

<sup>5</sup>School of Medicine, Shenzhen Campus of Sun Yat-sen University, Sun Yat-Sen University, Shenzhen, China

<sup>6</sup>Department of Surgical Oncology and General Surgery, The First Hospital of China Medical University, Shenyang, China

<sup>7</sup>School of Electronics and Communication Engineering, Shenzhen Campus of Sun Yat-sen University, Sun Yat-Sen University, Shenzhen, China

Received: 18 September 2024 / Accepted: 18 February 2025

Published online: 01 March 2025

## References

1. Cossu G, Birchall M, Brown T, De Coppi P, Culme-Seymour E, Gibbon S, Hitchcock J, Mason C, Montgomery J, Morris S, et al. Commission: stem cells and regenerative medicine. *Lancet*. 2018;391(10123):883–910.
2. Yoshimoto Y, Oishi Y. Mechanisms of skeletal muscle-tendon development and regeneration/healing as potential therapeutic targets. *Pharmacol Ther*. 2023;243:108357.
3. Chazaud B. Inflammation and skeletal muscle regeneration: leave it to the macrophages! *Trends Immunol*. 2020;41(6):481–92.
4. Espino-Gonzalez E, Dalbram E, Mounier R, Gondin J, Farup J, Jessen N, Trebak JT. Impaired skeletal muscle regeneration in diabetes: from cellular and molecular mechanisms to novel treatments. *Cell Metabol*. 2024;36(6):1204–36.



5. Zhang H, Ryu D, Wu Y, Gariani K, Wang X, Luan P, D'Amico D, Ropelle ER, Lutolf MP, Aebersold R, et al. NAD<sup>+</sup> repletion improves mitochondrial and stem cell function and enhances life span in mice. *Science*. 2016;352(6292):1436–43.
6. Giordani L, He GJ, Negroni E, Sakai H, Law JYC, Siu MM, Wan R, Corneau A, Tajbakhsh S, Cheung TH, et al. High-Dimensional Single-Cell cartography reveals novel skeletal Muscle-Resident cell populations. *Mol Cell*. 2019;74(3):609–e621606.
7. Saito Y, Chikenji TS, Matsumura T, Nakano M, Fujimiya M. Exercise enhances skeletal muscle regeneration by promoting senescence in fibro-adipogenic progenitors. *Nat Commun*. 2020;11(1):889.
8. Lukjanenko L, Karaz S, Stuelsatz P, Gurriaran-Rodriguez U, Michaud J, Damme G, Sizzano F, Mashinchian O, Ancel S, Migliavacca E, et al. Aging disrupts muscle stem cell function by impairing matricellular WISP1 secretion from Fibro-Adipogenic progenitors. *Cell Stem Cell*. 2019;24(3):433–e446437.
9. Peng JY, Han LL, Liu B, Song JW, Wang Y, Wang KP, Guo Q, Liu XY, Li Y, Zhang JJ et al. Gli1 marks a Sentinel muscle stem cell population for muscle regeneration. *Nat Commun*. 2023, 14(1).
10. Jiang H, Liu B, Lin J, Xue T, Han Y, Lu C, Zhou S, Gu Y, Xu F, Shen Y, et al. MuSCs and IPCs: roles in skeletal muscle homeostasis, aging and injury. *Cell Mol Life Sci*. 2024;81(1):67.
11. Relaix F, Bencze M, Borok MJ, Der Vartanian A, Gattazzo F, Mademtzoglou D, Perez-Diaz S, Prola A, Reyes-Fernandez PC, Rotini A, et al. Perspectives on skeletal muscle stem cells. *Nat Commun*. 2021;12(1):692.
12. Wu J, Ren B, Wang D, Lin H. Regulatory T cells in skeletal muscle repair and regeneration: recent insights. *Cell Death Dis*. 2022;13(8):680.
13. Wosczyzna MN, Konishi CT, Perez Carbajal EE, Wang TT, Walsh RA, Gan Q, Wagner MW, Rando TA. Mesenchymal stromal cells are required for regeneration and homeostatic maintenance of skeletal muscle. *Cell Rep*. 2019;27(7):2029–35. e2025.
14. Contreras O, Rossi FMV, Theret M. Origins, potency, and heterogeneity of skeletal muscle fibro-adipogenic progenitors-time for new definitions. *Skelet Muscle*. 2021;11(1):16.
15. Uezumi A, Fukada S, Yamamoto N, Takeda S, Tsuchida K. Mesenchymal progenitors distinct from satellite cells contribute to ectopic fat cell formation in skeletal muscle. *Nat Cell Biol*. 2010;12(2):143–52.
16. Scott RW, Arostegui M, Schweitzer R, Rossi FMV, Underhill TM. Hic1 defines quiescent mesenchymal progenitor subpopulations with distinct functions and fates in skeletal muscle regeneration. *Cell Stem Cell*. 2019;25(6):797–e813799.
17. Molina T, Fabre P, Dumont NA. Fibro-adipogenic progenitors in skeletal muscle homeostasis, regeneration and diseases. *Open Biol*. 2021;11(12):210110.
18. Petrilli LL, Spada F, Palma A, Reggio A, Rosina M, Gargioli C, et al. High-dimensional single-cell quantitative profiling of skeletal muscle cell population dynamics during regeneration. *Cells*. 2020;9(7).
19. Joe AW, Yi L, Natarajan A, Le Grand F, So L, Wang J, Rudnicki MA, Rossi FM. Muscle injury activates resident fibro/adipogenic progenitors that facilitate myogenesis. *Nat Cell Biol*. 2010;12(2):153–63.
20. Yin K, Zhang CM, Deng ZH, Wei XY, Xiang TW, Yang C, Chen C, Chen YQ, Luo F. FAPs orchestrate homeostasis of muscle physiology and pathophysiology. *Faseb J*. 2024, 38(24).
21. Chen W, You W, Valencak TG, Shan T. Bidirectional roles of skeletal muscle fibro-adipogenic progenitors in homeostasis and disease. *Ageing Res Rev*. 2022;80:101682.
22. Hardy D, Besnard A, Latil M, Jouvion G, Briand D, Thépenier C, Pascal Q, Guignin A, Gayraud-Morel B, Cavaillon JM et al. Comparative study of injury models for studying muscle regeneration in mice. *PLoS ONE*. 2016, 11(1).
23. Feng F, Cui BQ, Fang L, Lan T, Luo K, Xu X, Lu ZB. DDAH1 protects against Cardiotoxin-Induced muscle injury and regeneration. *Antioxidants-Basel*. 2023, 12(9).
24. Czerwinska AM, Streminska W, Ciemerych MA, Grabowska I. Mouse gastrocnemius muscle regeneration after mechanical or cardiotoxin injury. *Folia Histochem Cyto*. 2012;50(1):144–53.
25. Wang Y, Lu J, Liu Y. Skeletal muscle regeneration in Cardiotoxin-Induced muscle injury models. *Int J Mol Sci*. 2022, 23(21).
26. Aierken A, Li B, Liu P, Cheng X, Kou Z, Tan N, Zhang M, Yu S, Shen Q, Du X, et al. Melatonin treatment improves human umbilical cord mesenchymal stem cell therapy in a mouse model of type II diabetes mellitus via the PI3K/AKT signaling pathway. *Stem Cell Res Ther*. 2022;13(1):164.
27. Hao YH, Hao S, Andersen-Nissen E, Mauck WM, Zheng SW, Butler A, Lee MJ, Wilk AJ, Darby C, Zager M, et al. Integrated analysis of multimodal single-cell data. *Cell*. 2021;184(13):3573–.
28. Ziegenhain C, Vieth B, Parekh S, Reinius B, Guillaumet-Adkins A, Smets M, Leonhardt H, Heyn H, Hellmann I, Enard W. Comparative analysis of Single-Cell RNA sequencing methods. *Mol Cell*. 2017;65(4):631–e643634.
29. Xie C, Mao X, Huang J, Ding Y, Wu J, Dong S, Kong L, Gao G, Li CY, Wei L. KOBAS 2.0: a web server for annotation and identification of enriched pathways and diseases. *Nucleic Acids Res*. 2011;39(Web Server issue):W316–322.
30. Yang J, Chen L, Kong X, Huang T, Cai YD. Analysis of tumor suppressor genes based on gene ontology and the KEGG pathway. *PLoS ONE*. 2014;9(9):e107202.
31. Chen L, Zhang YH, Lu G, Huang T, Cai YD. Analysis of cancer-related lncRNAs using gene ontology and KEGG pathways. *Artif Intell Med*. 2017;76:27–36.
32. Te LJI, Doherty C, Correa J, Batt J. Identification, isolation, and characterization of fibro-adipogenic progenitors (FAPs) and myogenic progenitors (MPs) in skeletal muscle in the rat. *J Vis Exp*. 2021;(172):10.3791/61750.
33. Su CM, Tsai CH, Chen HT, Wu YS, Chang JW, Yang SF, Tang CH. Melatonin improves muscle injury and differentiation by increasing Pax7 expression. *Int J Biol Sci*. 2023;19(4):1049–62.
34. Yui PB, Hong CC, Sachidanandan C, Babbitt JL, Deng DY, Hoyng SA, Lin HY, Bloch KD, Peterson RT. Dorsomorphin inhibits BMP signals required for embryogenesis and iron metabolism. *Nat Chem Biol*. 2008;4(1):33–41.
35. Di S, Wang Z, Hu W, Yan X, Ma Z, Li X, Li W, Gao J. The protective effects of melatonin against LPS-Induced septic myocardial injury: A potential role of AMPK-Mediated autophagy. *Front Endocrinol (Lausanne)*. 2020;11:162.
36. Ledolter J, Gramlich OW, Kardon RH. Parametric statistical inference for comparing means and variances. *Invest Ophthalmol Vis Sci*. 2020;61(8):25.
37. Wei X, Nicoletti C, Puri PL. Fibro-Adipogenic progenitors: versatile keepers of skeletal muscle homeostasis, beyond the response to myotrauma. *Semin Cell Dev Biol*. 2021;119:23–31.
38. Sastourné-Arrey Q, Mathieu M, Contreras X, Monferran S, Bourlier V, Gil-Ortega M, Murphy E, Laurens C, Varin A, Guissard C et al. Adipose tissue is a source of regenerative cells that augment the repair of skeletal muscle after injury. *Nat Commun*. 2023, 14(1).
39. Brillo V, Chieragato L, Leanza L, Muccioli S, Costa R. Mitochondrial dynamics, ROS, and cell signaling: A blended overview. *Life-Basel*. 2021, 11(4).
40. Pévet P. Melatonin. *Dialogues Clin Neurosci*. 2002;4(1):57–72.
41. Steinberg GR, Hardie DG. New insights into activation and function of the AMPK. *Nat Rev Mol Cell Bio*. 2023;24(4):255–72.
42. Giuliani G, Rosina M, Reggio A. Signaling pathways regulating the fate of fibro/adipogenic progenitors (FAPs) in skeletal muscle regeneration and disease. *Febs J*. 2022;289(21):6484–517.
43. Nawaz A, Bilal M, Fujisaka S, Kado T, Aslam MR, Ahmed S, Okabe K, Igarashi Y, Watanabe Y, Kuwano T, et al. Depletion of CD206(+) M2-like macrophages induces fibro-adipogenic progenitors activation and muscle regeneration. *Nat Commun*. 2022;13(1):7058.
44. Reggio A, Rosina M, Palma A, Perpetuini AC, Petrilli LL, Gargioli C, Fuoco C, Micarelli E, Giuliani G, Cerretani M, et al. Adipogenesis of skeletal muscle fibro/adipogenic progenitors is affected by the WNT5a/GSK3/β-catenin axis. *Cell Death Differ*. 2020;27(10):2921–41.
45. Di Micco R, Krizhanovsky V, Baker D, di Fagagna FD. Cellular senescence in ageing: from mechanisms to therapeutic opportunities. *Nat Rev Mol Cell Bio*. 2021;22(2):75–95.
46. Zhang L, Pitcher LE, Yousefzadeh MJ, Niedernhofer LJ, Robbins PD, Zhu Y. Cellular senescence: a key therapeutic target in aging and diseases. *J Clin Invest*. 2022, 132(15).
47. Englund DA, Zhang X, Aversa Z, LeBrasseur NK. Skeletal muscle aging, cellular senescence, and senotherapeutics: current knowledge and future directions. *Mech Ageing Dev*. 2021;200:111595.
48. Uezumi A, Ikemoto-Uezumi M, Zhou H, Kurosawa T, Yoshimoto Y, Nakatani M, Hitachi K, Yamaguchi H, Wakatsuki S, Araki T et al. Mesenchymal Bmp3b expression maintains skeletal muscle integrity and decreases in age-related sarcopenia. *J Clin Invest*. 2021, 131(1).
49. Kang X, Yang MY, Shi YX, Xie MM, Zhu M, Zheng XL, Zhang CK, Ge ZL, Bian XT, Lv JT, et al. Interleukin-15 facilitates muscle regeneration through modulation of fibro/adipogenic progenitors. *Cell Commun Signal*. 2018;16(1):42.
50. Quinn LS, Strait-Bodey L, Anderson BG, Argilés JM, Havel PJ. Interleukin-15 stimulates adiponectin secretion by 3T3-L1 adipocytes: evidence for a skeletal muscle-to-fat signaling pathway. *Cell Biol Int*. 2005;29(6):449–57.
51. Stacchiotti A, Favero G, Rodella LF. Impact of melatonin on skeletal muscle and exercise. *Cells*. 2020, 9(2).
52. Jauhari A, Baranov SV, Suofu Y, Kim J, Singh T, Yablonska S, Li F, Wang X, Oberly P, Minnigh MB, et al. Melatonin inhibits cytosolic mitochondrial DNA-induced

- neuroinflammatory signaling in accelerated aging and neurodegeneration. *J Clin Invest.* 2020;130(6):3124–36.
53. Zhang Y, Wang Y, Xu J, Tian F, Hu S, Chen Y, Fu Z. Melatonin attenuates myocardial ischemia-reperfusion injury via improving mitochondrial fusion/mitophagy and activating the AMPK-OPA1 signaling pathways. *J Pineal Res.* 2019;66(2):e12542.
54. Acuña-Castroviejo D, Escames G, López LC, Hitos AB, León J. Melatonin and nitric oxide: two required antagonists for mitochondrial homeostasis. *Endocrine.* 2005;27(2):159–68.
55. Posadzki PP, Bajpai R, Kyaw BM, Roberts NJ, Brzezinski A, Christopoulos GI, et al. Melatonin and health: an umbrella review of health outcomes and biological mechanisms of action. *BMC Med.* 2018;16(1):18.
56. Garcia D, Shaw RJ. AMPK: mechanisms of cellular energy sensing and restoration of metabolic balance. *Mol Cell.* 2017;66(6):789–800.
57. Herzig S, Shaw RJ. AMPK: guardian of metabolism and mitochondrial homeostasis. *Nat Rev Mol Cell Biol.* 2018;19(2):121–35.
58. Hsu CC, Peng D, Cai Z, Lin HK. AMPK signaling and its targeting in cancer progression and treatment. *Semin Cancer Biol.* 2022;85:52–68.

### Publisher's note

Springer Nature remains neutral with regard to jurisdictional claims in published maps and institutional affiliations.